ROYAL SOCIETY OF CHEMISTRY

## EDGE ARTICLE

Check for updates

# Multifunctional oxadiazole-based ultraviolet-emitting materials used as hosts for multicolor phosphorescence†

Lizhi Chu,[a] Chenglin Ma,[a] Li Zhang,[a] Yannan Zhou,[a] Jingru Song,[a] Qikun Sun,[a] Shi-Tong Zhang,*[b] Wenjun Yang [ID][a] and Shanfeng Xue [ID]*[a]

Highly efficient ultraviolet materials and host materials for organic light-emitting diodes (OLEDs) have been gaining increasing attention in recent years. In this study, three donor–acceptor (D–A) molecules with different HLCT properties were designed and synthesized using oxadiazole as an electron acceptor. Not only does the molecule *m*-PIOXZ exhibit efficient ultraviolet electroluminescence, but it can also serve as the host material for high-efficiency phosphorescent OLEDs (PhOLEDs) with low roll-off. As a result, high external quantum efficiency (EQE) and long operational lifetimes are obtained in green, yellow and red emissive PhOLEDs, providing new insights for developing high-efficiency, low roll-off, and full-color OLEDs.

## Introduction

Organic light-emitting diodes (OLEDs) have gained a large share in the display and lighting markets due to the advantages of wide color gamut, wide viewing angles and suitability for ultra-thin and flexible displays.[1–4] In particular, ultraviolet-emissive materials are attracting increasing attention due to their bi-functionality as both emitters and potential host materials for fluorescent OLEDs (FOLEDs) and phosphorescent OLEDs (PhOLEDs). However, highly efficient ultraviolet OLEDs are seldom reported because of the high injection barrier and insufficient carrier transportation due to their wide band gap.[5–9] Therefore, it is crucial to figure out the rational molecular design method for the bi-functional ultraviolet emissive material.

The most important barrier that prevents ultraviolet light-emitting materials from practical application is the very large band gap, which results in difficult carrier injection and reduced maximum external quantum efficiency (EQE$_{max}$).[10–12] Recently, the bipolar donor–acceptor (D–A) structure has been proposed to solve the above problem of ultraviolet emissive materials. The various options of donor and acceptor moieties help effectively tune the energy gap between the highest occupied molecular orbital (HOMO) and the lowest unoccupied molecular orbital (LUMO), guaranteeing ultraviolet emission.[13–17] However, in terms of the molecular design of ultraviolet electroluminescent materials, the balancing of locally-excited (LE) and charge-transfer (CT) excited states is quite difficult: CT excitons are always of low energy, but they are still needed for improving the exciton utilization efficiency (EUE) in OLEDs.[18] To solve this problem, the hybridized local and charge-transfer (HLCT) excited state has been explored. For example, Zhong *et al.* designed and synthesized a high-performance ultraviolet OLED based on a high steric hindrance structure, which emits ultraviolet light at 396 nm with Commission Internationale de lEclairage (CIE) coordinates of (0.160, 0.045), and a maximum external quantum efficiency (EQE$_{max}$) of 7.9%.[19] More importantly, the molecular design of spatially separated donor and acceptor moieties can guarantee independent carrier transportation channels, enabling their potential application as efficient host materials for phosphorescent OLEDs.[20–23] As a result, although several studies on such dual-function materials have been reported,[24–29] different combinations and linkages of donor and acceptor moieties can result in different excited state properties, and the research on the structure–property relationship, especially how to control or balance the LE and CT excited states is still rare. Therefore, it is important to develop more potential molecular structures as well as figure out the structure–property relationship in terms of their excited state properties.

In this study, we designed three D–A structures with large HOMO–LUMO band-gaps to realize highly efficient ultraviolet-

[a]Key Laboratory of Rubber-Plastics of the Ministry of Education, School of Polymer Science & Engineering, Qingdao University of Science and Technology, 53-Zhengzhou Road, Qingdao 266042, P. R. China. E-mail: sfxue@qust.edu.cn

[b]State Key Laboratory of Supramolecular Structure and Materials, Institute of Theoretical Chemistry, College of Chemistry, Jilin University, Changchun 130012, P. R. China. E-mail: stzhang@jlu.edu.cn
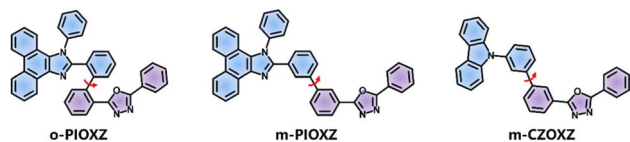
Fig. 1 The molecular structures of *m*-PIOXZ, *o*-PIOXZ, and *m*-CZOXZ.

emissive and host materials (*o*-PIOXZ, *m*-PIOXZ, and *m*-CZOXZ, Fig. 1). The phenanthroimidazole group contains both sp² and sp³ hybridized nitrogen atoms, allowing it to be used both as an electron donor and an electron acceptor. Additionally, the phenanthroimidazole group has a large planar shape, which contributes to its good carrier transport performance.[30–33] Carbazole has a high triplet energy level and excellent hole transport performance, making it a common functional group in host materials.[34–38] As an electron acceptor, oxadiazole exhibits strong electron-withdrawing ability due to the presence of nitrogen and oxygen heteroatoms. Moreover, oxadiazole has good electron transport properties, making it a common material for electron transport layers in OLED devices.[39,40] In order to break the conjugation of the molecule and achieve a high triplet energy level, *o*-PIOXZ with a large twisted structure was first designed and synthesized by connecting phenanthroimidazole and oxadiazole. Considering that excessively twisted molecules are difficult to stack effectively and thus generate a good carrier transport channel, the meta-connected *m*-PIOXZ was synthesized. At the same time, to further improve the triplet energy level and enhance hole transport performance, *m*-CZOXZ with a meta-linker between carbazole and oxadiazole was designed and synthesized. Among the three materials, the non-doped device with the LE state *m*-PIOXZ as the light-emitting layer has a short-wavelength emission at 404 nm, CIE coordinates of (0.160, 0.045), and an EQE$_{max}$ of 5.23%, which exceeds the theoretical maximum of the spin-statistics limit, due to its hybridized local and charge-transfer (HLCT) excited state properties. Furthermore, green, yellow, and red PhOLEDs using *m*-PIOXZ as the host material demonstrated excellent performance, with maximum external quantum efficiencies (EQE$_{max}$) of 25.20%, 29.61%, and 21.38%, maximum power efficiencies (PE$_{max}$) of 102.34 lm W⁻¹, 105.63 lm W⁻¹, and 40.71 lm W⁻¹, and efficiency roll-offs of 1.15%, 2.36%, and 6.87% at 1000 cd m⁻², respectively, which are all among the best results that have been reported.

# Results and discussion

## Synthesis and characterization

The structures of the three molecules are shown in Fig. 1. The products were obtained by Debus one-pot synthesis and Suzuki coupling reactions. The materials were characterized by ¹H and ¹³C nuclear magnetic resonance (NMR) and mass spectrometry. The detailed synthesis routes (Scheme S1†) and structural characterization data (Fig. S1–S9) are presented in the ESI.† The thermal stability of the three materials was measured by thermogravimetric analysis (TGA) and differential scanning calorimetry (DSC). As shown in Fig. S10,† based on TGA, the thermal decomposition temperatures ($T_d$, at 5% weight loss) for the three materials *o*-PIOXZ, *m*-PIOXZ, and *m*-CZOXZ are 341 °C, 411 °C, and 343 °C, respectively, indicating high thermal stability. The glass transition temperatures ($T_g$) of the three materials are 115 °C, 114 °C, and 78 °C (Fig. S11†), respectively, demonstrating good morphological stability. The electrochemical properties of the three materials were tested using cyclic voltammetry (CV). As shown in Fig. S12† and Table 1, the band-gaps between the HOMO and LUMO of the three molecules are estimated to be 3.25 eV, 3.27 eV, and 3.22 eV, respectively, meeting with the demand for a wide band-gap and ultraviolet emission.

## Molecular design and theoretical calculations

To understand the excited states of these compounds, density functional theory (DFT) and time-dependent DFT (TDDFT) calculations were performed at the PBE0/6-31g(d,p) and BMK/6-31g(d,p) levels using Gaussian 09 software[41,42] (Fig. 2 and S13–S15†). First, due to the large spatial hindrance of the ortho-substitution, the dihedral angle between the donor and acceptor units of *o*-PIOXZ is 74.77°, which is twice that of *m*-PIOXZ and *m*-CZOXZ (38.95° and 38.35°, respectively). However, no matter how large or small the torsion angles are, the ground state HOMO/LUMO of the three materials show similar separated orbital patterns, corresponding to separated donor and acceptor functional units for both hole and electron injection, which is favorable for the molecular design of bipolar host materials. As for the S₁ excited state natural transition orbital (NTO), due to the lower donor ability of phenanthroimidazole, there is no efficient charge-transfer (CT) character found in *o*-PIOXZ and *m*-PIOXZ. In contrast, carbazole substituted *m*-CZOXZ shows typical hybridized local and charge-transfer (HLCT) excited state properties in its S₁ state: the NTO hole is

Table 1 Photophysical properties, energy levels, and thermal stabilities of bipolar materials

| Molecules | HOMO/LUMO[a] [eV] | $E_g$[b] [eV] | $\lambda_{abs}$ [nm] sol.[c] | $\lambda_{PL}$ [nm] sol. /film[c] | $\Phi_{PL}$ [%] sol. /film[c] | $E_{S_1}/E_{T_1}$[d] [eV] | $T_g/T_m/T_d$[e] [°C] |
|---|---|---|---|---|---|---|---|
| *o*-PIOXZ | −5.60/−2.35 | 3.25 | 257 | 421/417 | 98.9/20.5 | 3.51/2.89 | 155/251/341 |
| *m*-PIOXZ | −5.50/−2.23 | 3.27 | 261 | 371/404 | 99.4/40.4 | 3.49/2.73 | 144/241/411 |
| *m*-CZOXZ | −5.62/−2.40 | 3.22 | 288 | 349/391 | 22.5/19.1 | 3.67/2.90 | 78/156/343 |

[a] Determined from cyclic voltammetry measurement. [b] The bandgap energy was estimated from the electrochemical bandgap. [c] Measured in THF solution (10⁻⁵ M). [d] The S₁/T₁ energy levels were estimated from the highest energy vibration subband of the fluorescence and phosphorescence in THF at 77 K. [e] Glass transition temperatures, melting temperatures and temperatures corresponding to 5% weight loss.
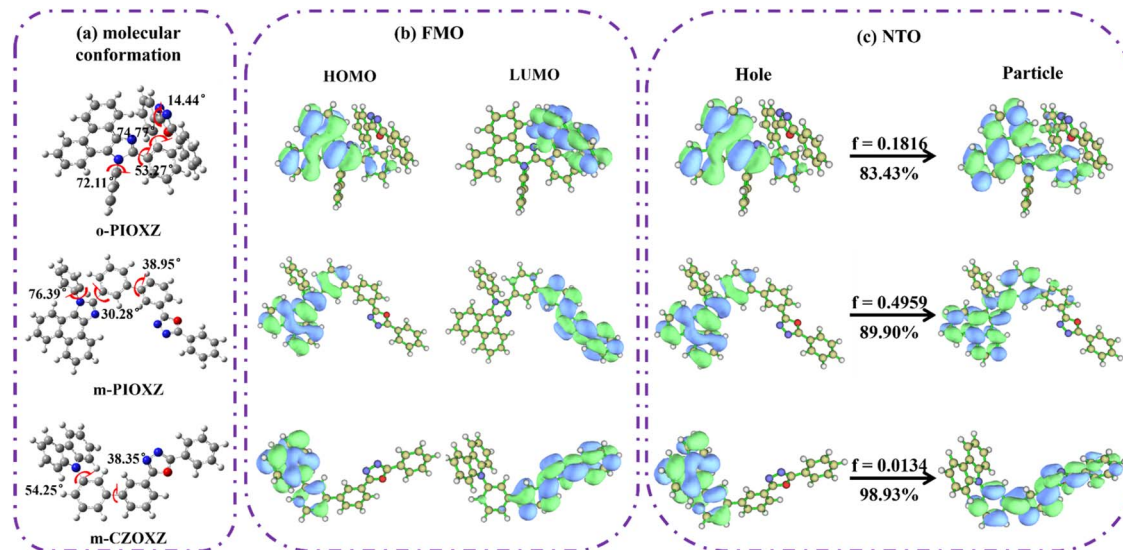
Fig. 2 (a) The geometries and structural formulae, (b) the frontier orbital distribution, and (c) the $S_0 \rightarrow S_1$ natural transition orbital (NTO) of the three materials.

mainly located on the carbazole donor, while the NTO particle is located on the oxadiazole acceptor, with an obvious overlap on the linking benzene ring of donor and acceptor units.

## Photophysical properties

The UV-vis absorption and photoluminescence (PL) spectra of the three materials in diluted THF ($10^{-5}$ mol L$^{-1}$) and neat films at room temperature are shown in Fig. 3 and Table 1. The maximum absorption peaks of *o*-PIOXZ and *m*-PIOXZ are around 260 nm, attributed to the phenanthroimidazole absorption. Besides this, *o*-PIOXZ possesses a shoulder peak at about 288 nm, which can be attributed to the CT absorption, while *m*-PIOXZ does not show this shoulder peak due to the meta-linkage enhanced conjugation. However, despite the similar meta-linkage, *m*-CZOXZ shows a similar CT-like wide absorption band to *o*-PIOXZ at 287 nm, revealing that the

stronger donor ability of carbazole can also contribute to the formation of the CT excited state. Notably, *m*-CZOXZ also shows vibrational fine structure in PL spectra in low polarity solvents, indicating the hybridization of LE and CT excited state components. The corresponding Lippert–Mataga solvatochromic models of the three materials further reveal their distinct excited state properties, as shown in Fig. 4. The excited-state dipole moment ($\mu_e$) of the LE-like *m*-PIOXZ is only 5.39 Debye, while the CT-like *o*-PIOXZ shows a large $\mu_e$ of 15 Debye in high polarity solvents. Interestingly, *m*-CZOXZ shows a very large $\mu_e$ of 35 Debye in high polarity solvents, while in lower polarity solvents, the $\mu_e$ falls to only 7 Debye, which can be assigned to the activated through-space CT in high polarity solvents, as the meta-linkage is not conjugate bonding. As a result, the neat film of *m*-PIOXZ shows the highest photoluminescence quantum yield (PLQY) of over 40% among the three materials, showing great potential in non-doped OLEDs. Additionally, the phosphorescent emissions of the three materials are also measured at nitrogen temperature with a delay time of 100 ms as shown in Fig. S17.† Thanks to the ultraviolet emission of the three materials, the $T_1$ levels of the three materials are all over 2.7 eV, enabling their applications as efficient host materials for green and red phosphorescent materials. From the transient PL spectrum, it can be seen that all three materials exhibit nanosecond lifetimes, as shown in Fig. S18.†
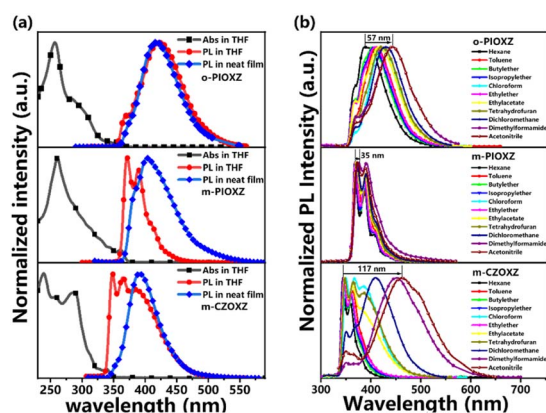


Fig. 3 (a) Normalized UV–vis absorption in THF solution ($10^{-5}$ M) and normalized PL spectra in THF ($10^{-5}$ M) and in the film state; (b) normalized PL spectra of the three materials in different solvents with increasing polarity.
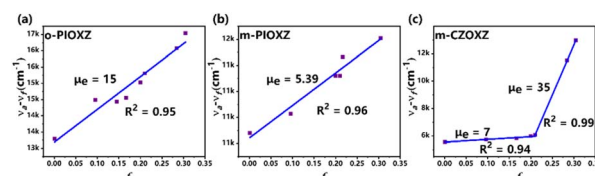


Fig. 4 The Lippert–Mataga solvatochromic model of (a) *o*-PIOXZ, (b) *m*-PIOXZ, and (c) *m*-CZOXZ.
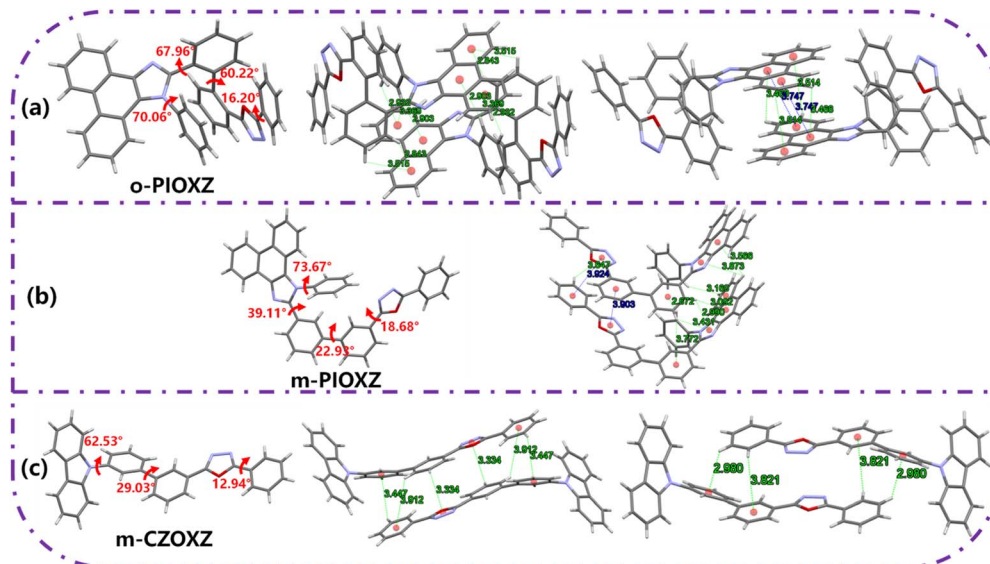
**Fig. 5** The molecular stacking patterns and single crystal structures with torsion angles of (a) *m*-PIOXZ, (b) *o*-PIOXZ and (c) *m*-CZOXZ.

## Single crystal structures and molecular stacking patterns

The stacking pattern of organic materials is crucial for their OLED performances in terms of the light-outcoupling ability and carrier transportation ability, especially when the materials are used as the host materials in the emitter layer. In order to investigate the stacking pattern of the three materials, single crystal growth is carried out on them, and three single crystals with good quality are obtained. As shown in Fig. 5, first, the twisting angles of the three molecules in the single crystal are all decreased compared to their optimized conformations in a vacuum, revealing that the intermolecular interactions in the three single crystals can give rise to the regular face-to-face stacking, which is crucial for light out-coupling and efficient

carrier transportation. For example, clear π stacking of phenanthroimidazole and oxadiazole can be found in *o*-PIOXZ and *m*-CZOXZ, respectively. However, this kind of stacking pattern is not an ideal one for the simultaneous transportation of holes and electrons: there is only donor (*o*-PIOXZ) or only acceptor (*m*-CZOXZ) packing in the single crystal, which may cause unbalanced transportation of holes and electrons in OLEDs. In contrast, the stacking pattern of *m*-PIOXZ is more ideal: both the donor phenanthroimidazole and the acceptor oxadiazole show clear π stacking. The formation of the ideal stacking can be understood by the relatively smaller bond twisting (approximately 39°, 23° and 19° for the marked bonds in Fig. 5b). We then fabricated the hole-only and electron-only devices for the three materials and investigated their carrier mobilities. As depicted in Fig. 6 and Table 2, *m*-PIOXZ shows the highest carrier mobilities (hole and electron mobilities of $5.1 \times 10^{-6}$ and $1.3 \times 10^{-5}$ cm$^2$ V$^{-1}$ s$^{-1}$, respectively). These values are also comparable to those of the traditional host or transportation materials such as CBP and mCP, which is in accordance with their regular, head-to-head stacking patterns. Notably, although balanced carrier transportation is not obtained in the other two materials, relatively high hole transportation (*o*-PIOXZ) and electron transportation (*m*-CZOXZ) are also obtained, corresponding to their regular face-to-face donor and acceptor stacking, respectively.
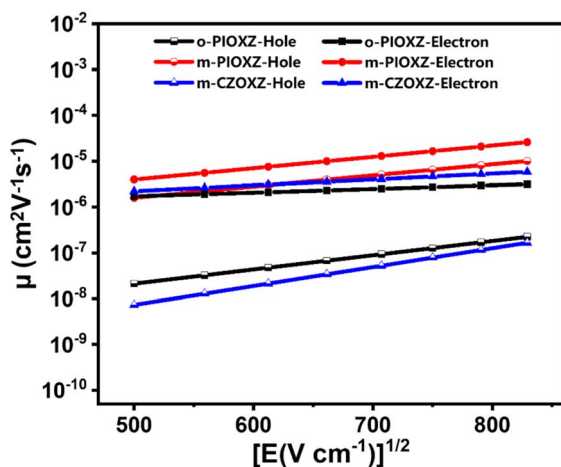


**Fig. 6** Electron field intensity–mobility curves. The hole-only device structure is ITO/HATCN (10 nm)/*m*-PIOXZ or *o*-PIOXZ or *m*-CZOXZ (80 nm)/HATCN (10 nm)/Al (100 nm), and the electron-only device structure is ITO/LiF (1 nm)/TPBi (10 nm)/*m*-PIOXZ, *o*-PIOXZ, *m*-CZOXZ (80 nm)/LiF (1 nm)/Al (100 nm).

**Table 2** The carrier mobility of the three materials under an electric field of $5.0 \times 10^5$ V cm$^{-1}$

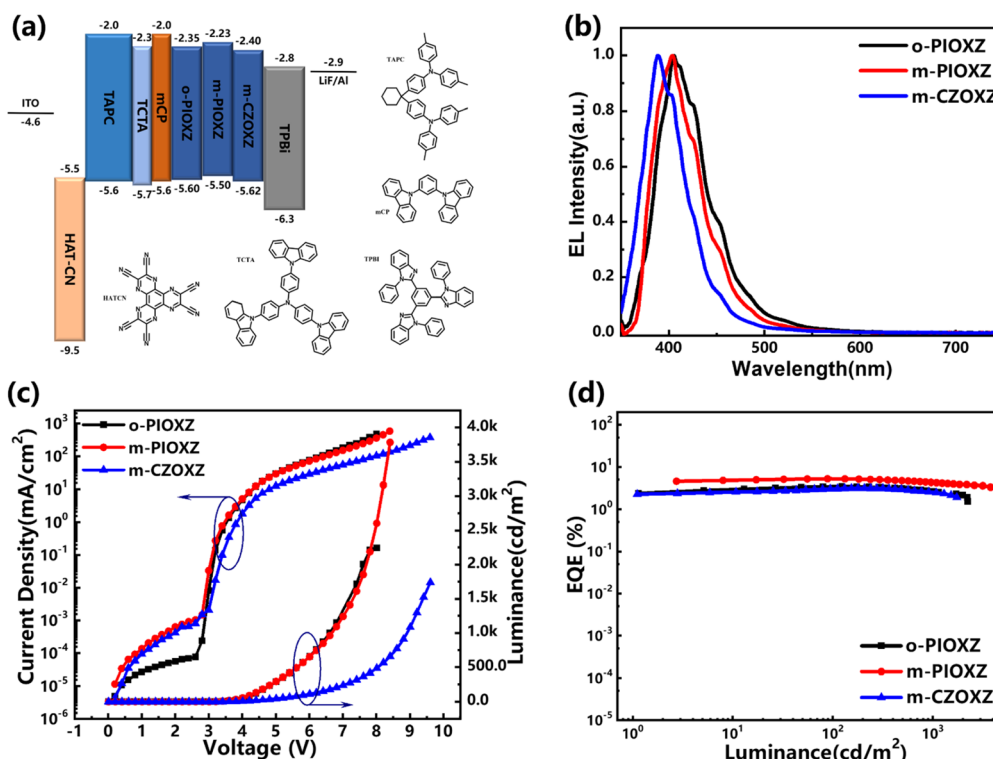| Compounds | Hole mobility [cm$^2$ V$^{-1}$ s$^{-1}$] | Electron mobility [cm$^2$ V$^{-1}$ s$^{-1}$] |
|---|---|---|
| *o*-PIOXZ | $9.3 \times 10^{-8}$ | $2.5 \times 10^{-6}$ |
| *m*-PIOXZ | $5.1 \times 10^{-6}$ | $1.3 \times 10^{-5}$ |
| *m*-CZOXZ | $5.2 \times 10^{-8}$ | $4.7 \times 10^{-6}$ |

Fig. 7  (a) Energy level diagrams; (b) EL spectra; (c) luminance–voltage–current density curves of non-doped OLEDs; and (d) external quantum efficiency–luminance curves.

Table 3   EL data of non-doped ultraviolet fluorescent OLEDs

| Emitters | $V_{on}^a$ [V] | $L_{max}^b$ [cd m$^{-2}$] | $CE_{max}^c$ [cd A$^{-1}$] | $PE_{max}^d$ [lm W$^{-1}$] | $EQE_{max}^e$ [%] | $\lambda_{EL}^f$ [nm] | CIE $(x, y)^g$ |
|---|---|---|---|---|---|---|---|
| o-PIOXZ | 3.2 | 2244 | 1.06 | 0.84 | 3.40 | 405 | (0.161, 0.056) |
| m-PIXOZ | 3.2 | 3782 | 1.08 | 0.99 | 5.23 | 404 | (0.160, 0.045) |
| m-CZOXZ | 3.6 | 1739 | 0.50 | 0.28 | 3.15 | 389 | (0.166, 0.047) |

[a] $V_{on}$ = turn-on voltage at 1 cd m$^2$. [b] $L_{max}$ = maximum luminance. [c] $CE_{max}$ = maximum current efficiency. [d] $PE_{max}$ = maximum power efficiency. [e] $EQE_{max}$ = maximum external quantum efficiency. [f] $\lambda_{EL}$ = peak of the electroluminescence spectrum. [g] CIE = CIE coordinates recorded at $EQE_{max}$.

## Electroluminescence performances

The electroluminescence performance of these three molecules as the EML in non-doped OLEDs was initially studied. The device structure was designed as follows: ITO/HATCN (20 nm)/TAPC (40 nm)/TCTA (5 nm)/mCP (5 nm)/EML (20 nm)/TPBi (35 nm)/LiF (1.5 nm)/Al (100 nm). Among them, ITO is used as the anode; HATCN (1,4,5,8,9,11-hexaazatriphenylenehexacarbonitrile) serves as the hole injection layer; TAPC (4,4′-cyclohexylidenebis[N,N-bis(p-tolyl)aniline]) and TCTA (4,4′,4″-tris(carbazol-9-yl)-triphenylamine) function as the hole transport layers; mCP (1,3-bis(carbazol-9-yl)benzene) acts as the electron blocking layer; TPBi (2,2′,2″-(1,3,5-benzinetriyl)-tris(1-phenyl-1-H-benzimidazole)) is used as both the electron transport layer and hole injection layer; LiF is used as the electron injection layer. The chemical structures and HOMO/LUMO energy levels of the different layers of the device are shown in Fig. 7. The data are summarized in Table 3.

First, all three devices show electroluminescence at around 400 nm, which is similar to their neat films and meets the demand of near-ultraviolet emission, revealing that the device structures are reasonable. Among the three non-doped OLEDs, m-PIOXZ exhibits the highest EQE of 5.23%, which is among the best results for non-doped ultraviolet OLEDs. This result can be first assigned to the balanced carrier mobilities of m-PIOXZ, which can be understood by the increased turn-on voltage of the m-CZOXZ non-doped OLED. Next, although m-PIOXZ is a LE material, the PLQY of m-PIOXZ is twice that of o-PIOXZ and m-CZOXZ (Table 1), which is also a key reason for the high EQE.

The simultaneously realized good hole and electron mobilities and the reasonable triplet energy level of m-PIOXZ further motivate us to investigate its application as an efficient host for phosphorescent OLEDs (PhOLEDs). The PhOLEDs were constructed using Ir(ppy)$_2$acac (bis[2-(2-pyridinyl-N)phenyl-C](acetylacetonato)iridium(III)), PO-01 (Iridium(III) bis(4-phenylthieno[3,2-c]pyridinato-N,C$_2$′)acetylacetonate), and Ir(MDQ)$_2$acac
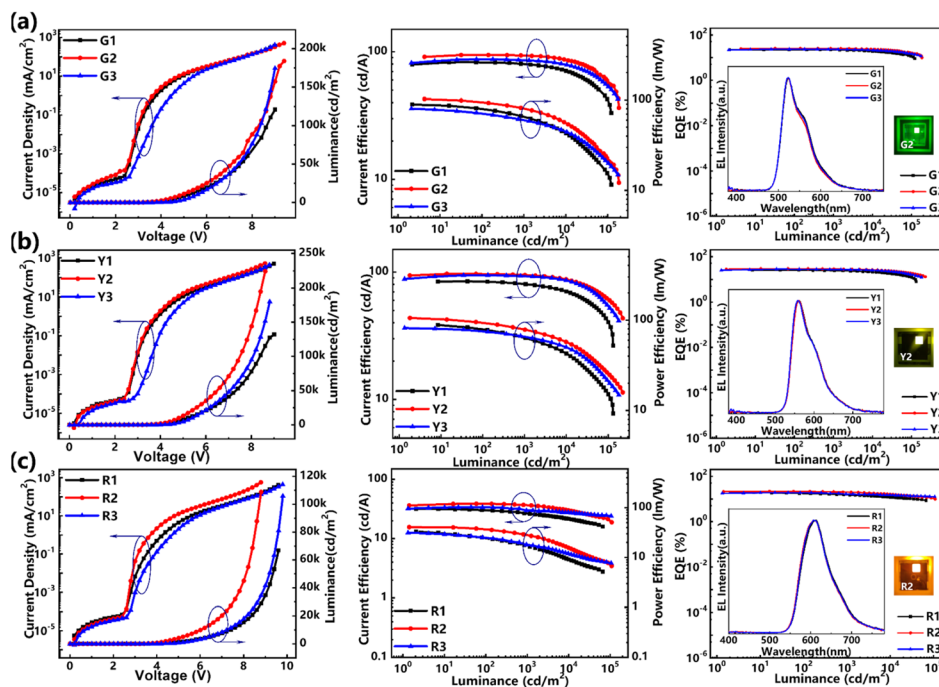
**Fig. 8** The current density–voltage–luminance curves, current efficiency–luminance–power efficiency curves, and EQE–luminance curves (inset: the EL spectrum and photograph of the operating devices) of the doped devices with (a–c) are green, yellow, and red PhOLEDs, respectively. o-PIOXZ, m-PIOXZ, and m-CZOXZ are the host materials for G1, G2, and G3, R1, R2, and R3, and Y1, Y2, and Y3 devices, respectively.

**Table 4** EL performance of PHOLEDs based on m-PIOXZ, o-PIOXZ, and m-CZOXZ hosts

| Devices[a] | $V_{on}{}^b$ [V] | $L_{max}{}^c$ [cd m$^{-2}$] | $CE_{max}{}^d$ [cd A$^{-1}$] | $PE_{max}{}^e$ [lm W$^{-1}$] | $EQE_{max}{}^f$ [%] | $EQE_{roll-off}{}^g$ [%] | $\lambda_{EL}{}^h$ [nm] | CIE$^i$ (x, y) |
|---|---|---|---|---|---|---|---|---|
| G1 | 2.8 | 121 192 | 82.68 | 89.07 | 22.29 | 3.05 | 524 | (0.33, 0.62) |
| G2 | 2.8 | 184 047 | 94.44 | 102.34 | 25.20 | 1.15 | 523 | (0.32, 0.63) |
| G3 | 3.2 | 174 659 | 87.18 | 80.25 | 23.27 | 1.49 | 523 | (0.32, 0.62) |
| Y1 | 3.0 | 132 085 | 84.61 | 88.34 | 25.99 | 5.40 | 562 | (0.48, 0.51) |
| Y2 | 2.8 | 224 515 | 96.91 | 105.63 | 29.61 | 2.36 | 561 | (0.48, 0.51) |
| Y3 | 3.4 | 179 917 | 94.54 | 81.60 | 28.64 | 2.56 | 559 | (0.47, 0.51) |
| R1 | 3.0 | 66 851 | 31.72 | 33.20 | 19.03 | 20.69 | 612 | (0.61, 0.38) |
| R2 | 2.8 | 108 781 | 38.78 | 40.71 | 21.38 | 6.87 | 608 | (0.60, 0.39) |
| R3 | 3.2 | 105 826 | 33.91 | 31.52 | 18.88 | 13.75 | 607 | (0.60, 0.39) |

$^a$ o-PIOXZ, m-PIOXZ, and m-CZOXZ are the host materials for G1, G2, and G3, Y1, Y2, and Y3, and R1, R2, and R3 devices, respectively. $^b$ $V_{on}$ = turn-on voltage at 1 cd m$^{-2}$. $^c$ $L_{max}$ = maximum luminance. $^d$ $CE_{max}$ = maximum current efficiency. $^e$ $PE_{max}$ = maximum power efficiency. $^f$ $EQE_{max}$ = maximum external quantum efficiency. $^g$ $EQE_{roll-off}$ = external quantum efficiency roll-off from the maximum value to 1000 cd m$^{-2}$. $^h$ $\lambda_{EL}$ = peak of the electroluminescence spectrum. $^i$ CIE = CIE coordinates recorded at $EQE_{max}$.

(bis(2-methyldibenzo[f,h]quinoxaline)(acetylacetonate)iridium(III)) as phosphorescent dopants for green, yellow, and red emission, respectively. The device structure of the PhOLED involves changing the EML in the undoped device to host: x wt% guest (where x = 8 for green and x = 3 for yellow and red). The test results are summarized in Fig. 8 and Table 4. We also fabricated the PhOLED using o-PIOXZ and m-CZOXZ as hosts for reference. First, as shown in Table 4, the turn-on voltage of the PhOLED with m-PIOXZ and o-PIOXZ as the host is lower than that of the doped devices with m-CZOXZ as the host, which is similar to those of their non-doped devices. Notably, the turn-on voltages of all PhOLEDs are lower than those of their non-doped OLEDs, especially, the turn-on voltages of PhOLEDs

related to m-PIOXZ are all as low as 2.8 V. More importantly, all three materials show efficient energy transfer to the phosphorescent guests in all PhOLEDs, revealing their abilities as host materials. (Fig. S20†).

Compared to the other two materials, m-PIOXZ possesses the best PhOLED performance, due to its satisfactory and balanced carrier mobilities. For example, the $L_{max}$, $CE_{max}$ and $PE_{max}$ of the green-doped device G2 reach 184 047 cd m$^{-2}$, 94.44 cd A$^{-1}$ and 102.34 lm W$^{-1}$, respectively; and the $EQE_{max}$ reaches 25.20%, which are excellent results compared to the previous reports.[22,28,35,43–46] More importantly, the efficiency roll-off at 1000 cd m$^{-2}$ of G2 is only 1.15% and the roll-off at 5000 cd m$^{-2}$ is only 4.81%, revealing that the device stability using m-PIOXZ

is expectable. The performance of PhOLEDs with these three molecules as host materials is better than that of traditional commercial host materials, such as CBP and mCP. The data are summarized in Fig. S21, S22, and Table S2.† Therefore, we further estimated the OLED operational lifetime of the G2 device. As shown in Fig. S23 and Table S1,† the operational lifetime of the G2 device reaches $LT_{50} = 67.75$ h at a luminance of 3548 cd m$^{-2}$ without encapsulation, corresponding to a 583 h lifetime at an initial luminance of 1000 cd m$^{-2}$, which is also a good result compared to the previous reports. Notably, not only the green OLED but also the yellow and red OLED Y2 and R2 using *m*-PIOXZ as host materials also obtain competitive performances in terms of the device efficiency, efficiency roll-off and operational lifetime. Last but not least, although *m*-PIOXZ is a LE molecule, the separated HOMOs/LUMOs and the effective stacking mode create a good hole–electron transport channel, balancing the carrier transport rate and facilitating efficient recombination of holes and electrons, which improves EL efficiency and reduces efficiency roll-off.

## Conclusion

In conclusion, three types of ultraviolet to deep-blue emissive molecules were synthesized and characterized. The donor–acceptor structure of these materials enables their dual functionality as ultraviolet-emitting materials and efficient hosts for phosphorescent dopants, particularly the meta-linked material *m*-PIOXZ. Green, yellow, and red PhOLEDs utilizing *m*-PIOXZ as the host achieve high efficiencies with EQE$_{max}$ exceeding 20% (low efficiency roll-off) and exhibit extended operational lifetimes, outperforming commercial host materials. These results highlight the significant potential of *m*-PIOXZ for practical applications.

## Data availability

The data supporting this article have been included as part of the ESI.† Additional data are available from the corresponding author upon reasonable request.

## Author contributions

L. Chu synthesized the materials, characterized their basic properties, performed data processing and analysis, and wrote the manuscript. C. Ma carried out the fabrication and characterization studies of the devices. L. Zhang, Y. Zhou, J. Song, and Q. Sun conducted data verification, reviewed and revised the article, and supervised the work. S.-T. Zhang supported the theoretical calculations. W. Yang provided financial support and supervised the work. S. Xue provided financial support, conceived the idea, and reviewed and edited the article.

## Conflicts of interest

The authors declare that they have no conflict of interest.

## Acknowledgements

## Notes and references

1 C. W. Tang and S. A. VanSlyke, *Appl. Phys. Lett.*, 1987, **51**, 913–915.

2 Y. Xu, P. Xu, D. Hu and Y. Ma, *Chem. Soc. Rev.*, 2021, **50**, 1030–1069.

3 P. Han, C. Lin, E. Xia, J. Cheng, Q. Xia, D. Yang, A. Qin, D. Ma and B. Z. Tang, *Angew. Chem., Int. Ed.*, 2023, **62**, e202310388.

4 U. Deori, G. P. Nanda, C. Murawski and P. Rajamalli, *Chem. Sci.*, 2024, **15**, 17739–17759.

5 J. Lou, G. Li, X. Guo, B. Li, D. Yang, H. Zhang, Z. Wang and B. Z. Tang, *Small*, 2024, **20**, 2308468.

6 H. Liu, Q. Bai, L. Yao, H. Zhang, H. Xu, S. Zhang, W. Li, Y. Gao, J. Li, P. Lu, H. Wang, B. Yang and Y. Ma, *Chem. Sci.*, 2015, **6**, 3797–3804.

7 X. He, J. Lou, B. Li, X. Dong, F. Zhong, W. Liu, X. Feng, D. Yang, D. Ma, Z. Zhao, Z. Wang and B. Z. Tang, *Adv. Mater.*, 2024, **36**, 2310417.

8 X. Guo, G. Li, J. Lou, K. Chen, R. Huang, D. Yang, H. Zhang, Z. Wang and B. Z. Tang, *Small*, 2022, **18**, 2204029.

9 B. Li, J. Lou, H. Zhang, G. Li, X. He, Y. Huang, N. Zheng, Z. Wang, D. Ma and B. Z. Tang, *Adv. Funct. Mater.*, 2023, **33**, 2212876.

10 P. Ma, Y. Chen, Y. Man, Q. Qi, Y. Guo, H. Wang, Z. Li, P. Chang, C. Qu, C. Han and H. Xu, *Angew. Chem., Int. Ed.*, 2024, **63**, e202316479.

11 Y. Luo, S. Li, Y. Zhao, C. Li, Z. Pang, Y. Huang, M. Yang, L. Zhou, X. Zheng, X. Pu and Z. Lu, *Adv. Mater.*, 2020, **32**, 2001248.

12 S. Liu, X. Zhang, C. Ou, S. Wang, X. Yang, X. Zhou, B. Mi, D. Cao and Z. Gao, *ACS Appl. Mater. Interfaces*, 2017, **9**, 26242–26251.

13 S.-L. Lin, L.-H. Chan, R.-H. Lee, M.-Y. Yen, W.-J. Kuo, C.-T. Chen and R.-J. Jeng, *Adv. Mater.*, 2008, **20**, 3947–3952.

14 Q. Li, Y. Guo, J. Lan, Y. Yang, D. Wu and Z. Bin, *Chem. Sci.*, 2024, **15**, 16096–16102.

15 K. E. Linton, A. L. Fisher, C. Pearson, M. A. Fox, L.-O. Pålsson, M. R. Bryce and M. C. Petty, *J. Mater. Chem.*, 2012, **22**, 11816–11825.

16 Y. Jia, Y. Zhang, S. Fan, S. Wu, X. Zhao, S. Wang and X. Li, *Org. Electron.*, 2019, **64**, 259–265.

17 H. Zhou, R. Wang, M. Sun, Y. Zhou, L. Zhang, J. Song, Q. Sun, S.-T. Zhang, W. Yang and S. Xue, *Chem. Sci.*, 2024, **15**, 18601–18607.

18 H. Zhang, B. Zhang, Y. Zhang, Z. Xu, H. Wu, P.-A. Yin, Z. Wang, Z. Zhao, D. Ma and B. Z. Tang, *Adv. Funct. Mater.*, 2020, **30**, 2002323.

19 Z. Zhong, X. Zhu, X. Wang, Y. Zheng, S. Geng, Z. Zhou, X. J. Feng, Z. Zhao and H. Lu, *Adv. Funct. Mater.*, 2022, **32**, 2112969.

20 C. Du, H. Liu, Z. Cheng, S. Zhang, Z. Qu, D. Yang, X. Qiao, Z. Zhao and P. Lu, *Adv. Funct. Mater.*, 2023, **33**, 2304854.

21 X. Zhan, Z. Wu, Y. Lin, Y. Xie, Q. Peng, Q. Li, D. Ma and Z. Li, *Chem. Sci.*, 2016, **7**, 4355–4363.

22 J. Xu, H. Liu, J. Li, Z. Zhao and B. Z. Tang, *Adv. Opt. Mater.*, 2021, **9**, 2001840.

23 C. Han, Z. Zhang, H. Xu, J. Li, G. Xie, R. Chen, Y. Zhao and W. Huang, *Angew. Chem., Int. Ed.*, 2012, **51**, 10104–10108.

24 W. Zhang, J. Yu, Q. Cao, Y. Qian, J. Wang, C. Yang, H. Zhuang, W. Bian, Y. Xin and X. Ban, *J. Mater. Chem. C*, 2023, **11**, 16247–16257.

25 M.-H. Tsai, Y.-H. Hong, C.-H. Chang, H.-C. Su, C.-C. Wu, A. Matoliukstyte, J. Simokaitiene, S. Grigalevicius, J. V. Grazulevicius and C.-P. Hsu, *Adv. Mater.*, 2007, **19**, 862–866.

26 Y. Tao, C. Yang and J. Qin, *Chem. Soc. Rev.*, 2011, **40**, 2943–2970.

27 X. Yang, G. Zhou and W.-Y. Wong, *Chem. Soc. Rev.*, 2015, **44**, 8484–8575.

28 C. Liu, T. Li, M. Sun, M. Xie, Y. Zhou, W. Feng, Q. Sun, S.-T. Zhang, S. Xue and W. Yang, *Adv. Funct. Mater.*, 2023, **33**, 2215066.

29 G.-X. Yang, J.-J. Zhu, S.-S. Tang, H.-J. Tan, X. He, J.-X. Jian, X.-H. Zheng and Q.-X. Tong, *Adv. Photonics Res.*, 2021, **2**, 2100031.

30 W. Cui, C. Liu, X. Chao, M. Xie, Q. Sun, D. Liu, Y. Pan, S.-T. Zhang, S. Xue and W. Yang, *Adv. Opt. Mater.*, 2023, **11**, 2202947.

31 P. Yu and Y. Xiao, *Materials*, 2021, **14**, 2349.

32 M. Sun, C. Ma, M. Xie, L. Chu, X. Wang, Q. Sun, W. Yang and S. Xue, *Org. Chem. Front.*, 2023, **10**, 4878–4886.

33 D. Sylvinson, H.-F. Chen, L. M. Martin, P. J. G. Saris and M. E. Thompson, *ACS Appl. Mater. Interfaces*, 2019, **11**, 5276–5288.

34 W.-C. Chen, Y. Yuan, S.-F. Ni, Q.-X. Tong, F.-L. Wong and C.-S. Lee, *Chem. Sci.*, 2017, **8**, 3599–3608.

35 W. Ma, Z. Bin, G. Yang, J. Liu and J. You, *Angew. Chem., Int. Ed.*, 2022, **61**, e202116681.

36 Q. Wang, F. Lucas, C. Quinton, Y.-K. Qu, J. Rault-Berthelot, O. Jeannin, S.-Y. Yang, F.-C. Kong, S. Kumar, L.-S. Liao, C. Poriel and Z.-Q. Jiang, *Chem. Sci.*, 2020, **11**, 4887–4894.

37 H. Sasabe, N. Toyota, H. Nakanishi, T. Ishizaka, Y.-J. Pu and J. Kido, *Adv. Mater.*, 2012, **24**, 3212–3217.

38 N. A. Kukhta, T. Matulaitis, D. Volyniuk, K. Ivaniuk, P. Turyk, P. Stakhira, J. V. Grazulevicius and A. P. Monkman, *J. Phys. Chem. Lett.*, 2017, **8**, 6199–6205.

39 Y. Tan, Z. Wang, C. Wei, Z. Liu, Z. Bian and C. Huang, *Org. Electron.*, 2019, **69**, 77–84.

40 Y.-T. Chang, J.-K. Chang, Y.-T. Lee, P.-S. Wang, J.-L. Wu, C.-C. Hsu, I.-W. Wu, W.-H. Tseng, T.-W. Pi, C.-T. Chen and C.-I. Wu, *ACS Appl. Mater. Interfaces*, 2013, **5**, 10614–10622.

41 T. Lu and F. Chen, *J. Comput. Chem.*, 2012, **33**, 580–592.

42 T. Lu and Q. Chen, *Chem. Methods*, 2021, **1**, 231–239.

43 B. Wang, X. Lv, J. Tan, Q. Zhang, Z. Huang, W. Yi and L. Wang, *J. Mater. Chem. C*, 2016, **4**, 8473–8482.

44 B. Patil, J. Lade, S.-S. Chiou, Y.-C. Cheng, Y.-F. Lin, Y. Jadhav, P. Chetti, C.-H. Chang and A. Chaskar, *Org. Electron.*, 2021, **92**, 106090.

45 B. Sun, K.-N. Tong, S.-N. Liu, M.-K. Fung and J. Fan, *J. Mater. Chem. C*, 2021, **9**, 2969–2976.

46 B. Sun, K.-N. Tong, X. Chen, J.-L. He, H. Liu, M.-K. Fung and J. Fan, *J. Mater. Chem. C*, 2021, **9**, 7706–7712.